Elucidation of the morphology of the hydrocarbon multi-block copolymer electrolyte membranes for proton exchange fuel cells

Yue Zhao,[1,*] Miru Yoshida,[2] Satoshi Koizumi,[3,*] Masahiro Rikukawa,[2]

Noemi Szekely,[4] Aurel Radulescu,[4] and Dieter Richter [5]

[1]*Quantum Beam Science Center (QuBS), Japan Atomic Energy Agency (JAEA), Watanuki-machi 1233, Takasaki, Gunma, 370-1292, Japan*

[2]*Department of Material Science, Sophia University, Tokyo, 102-0094, Japan*

[3]*Department of Engineering, Ibaraki University, Hitachi, 615-8510, Japan*

[4]*Forschungszentrum Jülich GmbH, Jülich Centre for Neutron Science @ MLZ, Lichtenbergstraße 1, D-85747 Garching, Germany*

[5]*Jülich Centre for Neutron Science & Institute for Complex Systems, Forschungszentrum Jülich GmbH, D-52425 Jülich, Germany*

*To whom all correspondence should be addressed at Yue Zhao (zhao.yue@jaea.go.jp); Satoshi Koizumi (skoizumi@mx.ibaraki.ac.jp)

ABSTRACT: We investigated the structure and the swelling behavior of two synthesized hydrocarbon polymer electrolyte membranes, made of multiblock copolymer poly(sulphonate phenylene)-*b*-poly(arylene ether ketone) with different block ratios, by using small-angle neutron scattering technique. A scattering maximum (ionomer peak) at high-q range ($0.1< q <0.3$ Å^{-1}) is shown commonly in both dry and wet states, with q being the magnitude of the scattering vector, while it shifts towards low-q region in the wet state due to the swelling of the ionomer domains with water. The swelling effect also results to a second scattering maximum in the middle-q range ($0.01< q <0.03$ Å^{-1}) because of the water-induced microphase separation. This swelling behavior was confirmed in various water mixtures of normal water and deuterated water with different volume ratios (contrast variation method). The morphology of the wet membranes was analyzed in terms of Hard-Sphere model with Percus-Yervick interference interactions. Our analysis indicated that (i) the hydrated microdomains in the membranes are interconnected, which is the key point to promote the proton conductivity; (ii) the water-induced microphase separation structure and the amphiphilicity of the matrix for embedding the ionomer domains are closely related to the chemical structure of the polymer.

Keywords: Small-angle neutron scattering (SANS), contrast variation, microphase separation, polymer electrolyte membrane (PEM)

I. Introduction

In the previous study, we reported the synthesis and characterization of a series of newly developed polymer electrolyte membranes (PEMs), made of multiblock copolymer poly(sulphonate phenylene)-*b*-poly(arylene ether ketone) $[PSP_x\text{-}b\text{-}PAEK_y]_n$ (see Figure 1) having different block ratios, ion exchange capacities (IEC), water uptake, and proton conductivity [1]. The studies indicated that in an optimal IEC range, these PEMs exhibit good dimensional stability at elevated operating temperatures with the proton conductivity comparable to the benchmark material Nafion. Since these PEMs were made up of hydrocarbon copolymers, the cost of the membranes is expected to be much lower than that of Nafion for the application in an industrial scale. The good properties of these PEMs on one hand are the results of the high glass transition temperature of the polymer, and on the other hand, are believed to be controlled by the microphase separation structures of the membranes in the hydrated state, though the precise manifestation of which was still unclear. In this work, we aim to advance this study and elucidate the hierarchical structures of these PEMs and understand the structure related unique properties such as the mechanical property and the proton conductivity.

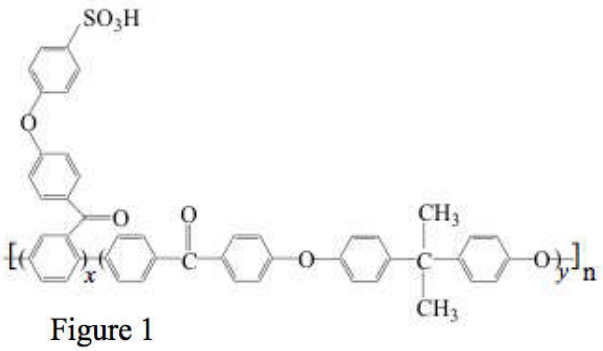

Figure 1

Proton Exchange Membrane Fuel Cells (PEMFCs) are considered to be the most versatile type of fuel cells currently in production [2-11], for their advantages such as low operating temperature, high current density, low weight, compactness, the potential for the long stack life, fast start-ups and etc [2-12]. These features make PEMFCs the most promising and attractive candidate for a wide variety of applications ranging from portable micropower and transportation to large-scale stationary power systems [2-8,11].

At the heart of PEMFCs is a proton conducting PEM, generally made from ionomers,

with the essential function of separating the electrodes and maintaining high intrinsic proton conductivity [2]. Ideal PEM material must satisfy demands such as high proton conductivity, good mechanical strength, high chemical and dimensional stabilities in the hydrated state [12-14]. So far, one of the most established and commercially available PEM materials is Nafion, developed by DuPont in 1960's. It is composed of a polytetrafluoroethylene backbone and perfluorinated pendant side chains terminated by sulfonic ionic groups, and has been used successfully as electrolyte polymer separators in many electrochemical devices [15,16]. However, perfluorinated PEMs have practical limitations such as decreased proton conductivity at high temperature and the high manufacturing cost. Therefore, it is of great significance to develop new PEM materials that can overcome the above drawbacks. For this purpose, numerous sulfonated aromatic hydrocarbon-type polymers such as poly(ether ether ketone) [17,18], poly(phenylene sulfone) [19], poly(arylene ether ketone) [20], polyimides [21], poly(phenylene) [22] and polybenzimidazole [23] were designed and synthesized in the past decade as alternatives to perfluorinated PEMs because of their rigid aromatic backbone, which gives them the potential of higher thermal stability and mechanical strength.

It is believed that the interesting properties of PEMs derive from the microphase separation of hydrophilic ionic material from the hydrophobic substance. Therefore, designing new PEMs should not only consider the architecture of the molecule itself, but also take the microphase-separated structure of the membrane into account. Various strategies including both approaches of synthesizing new polymers [17-23] and fabricating multilayered composite membrane [24] have been tried to control the microstructure of the PEMs. Recently, we have developed a hydrocarbon multiblock copolymer based on the poly(arylene ether ketone) (PAEK) backbone containing sulphonate phenylene (PSP) side chains (see Figure 1), where PAEK is hydrophobic and PSP is hydrophilic. Such a multiblock copolymer may form interconnected hydrophilic and hydrophobic microdomains, and possess many of the aforementioned properties [1]. The hydrophobic PAEK domains provide the mechanical

strength and constrain the dimensional changes of the materials upon swelling, while the hydrophilic PSP domains with proton transport channels promote the proton conductivity. Moreover, since the membrane is made up of hydrocarbon copolymers, the manufacturing cost is lowered.

To resolve the morphology of PEM materials, extensive theoretical and experimental studies have been reported [25-33], especially on the benchmark material such as Nafion. Its typical scattering pattern obtained from either small-angle neutron scattering (SANS) or small-angle X-ray scattering (SAXS) methods, includes a broad scattering maximum at high-q range [$q = (4\pi/\lambda)\sin(\theta/2)$, where λ and θ are the wavelength of the neutron (or X-ray) and the scattering angles, respectively.] around 0.1-0.2 $Å^{-1}$ (so-called "ionomer peak"), together with a scattering upturn at low-q range [26]. Though the structure of Nafion is still debated, there exists an overall consensus that hydrated sulfonic acid groups form phase separated morphologies in the nanometer regime, where water and sulfonic acid groups form spherical regions connected by water channels, embedded in the hydrophobic fluorocarbon matrix. These hydrated nanometer regimes have been referred to "ionic clusters", being proposed on the basis of the observations of the ionomer peak. The formation of these ionic clusters is believed to be the origin of the proton conductivity.

In this paper, we focus on the elucidation of the morphology of two $[PSP_x\text{-}b\text{-}PAEK_y]_n$ PEMs by using contrast variation SANS technique. The samples are designated as PSP_{14}-*b*-$PAEK_{14}$ and PSP_{28}-*b*-$PAEK_{14}$ for brevity, where the subscript 14 or 28 refers to the repeating unit number in each block. Obviously, the ratio of hydrophilic to hydrophobic blocks is different in these two samples, hence their IEC is also different. The characteristics of these two membranes can be found in Table 1. This paper is organized as follows: We first present the characterization of the swelling behavior of these two membranes equilibrated in D_2O (section III-1), and show the results of the solvent-contrast variation with respect to Hard-Sphere model analysis with Percus-Yervick interference approximation (section III-2).

Then we present discussion (section IV), in which we first propose the possible lamellar structure in the large length scale (section IV-1), then we justify whether the microdomains are interconnected in the middle-q range and propose the possible morphology models for both membranes (section IV-2). We then extend our discussion to the detailed and profound comparisons between experimentally extrapolated intensity and theoretically estimated intensity at q = 0, for the two membranes at all contrasts with respect to the morphologies mentioned in section IV-2, and confirm the morphology pattern for each membrane (section IV-3). Finally, in section IV-4 we present discussions on a possible interpretation of the physical origin of why the conductivity varies with polymer block ratio and what kind of structure plays an important role to control the conductivity. These discussions provide a profound and key insight into the interplay between the morphology and properties.

II. Experimental

II-1, Sample preparations. Two desired multiblock copolymers PSP_{14}-*b*-$PAEK_{14}$ and PSP_{28}-*b*-$PAEK_{14}$, were synthesized by varying the stoichiometry of the sulfonated monomers and hydrophobic oligomers via the nickel-catalyzed polymerization [1,34]. The molecular structure of these copolymers was determined by ^{1}H Nuclear magnetic resonance (NMR), Fourier transform infrared spectroscopy (FT-IR), Size exclusion chromatography (SEC) and elemental analysis, and shown in Figure 1 [1]. The characteristics of these two polymers were listed in Table 1.

The dry membranes with an average thickness of ~ 50 μm were prepared by solution casting onto a flat glass plate from its dimethyl sulfoxide solution with a concentration of 5 wt% [1]. Water swollen membranes were simply prepared by immersing the dry membranes into water at 25 ^{o}C. The water-uptake in the membranes, U, is determined by the weight measurements using eq. (1) below.

$$U = \frac{W_{wet} - W_{dry}}{W_{dry}} \qquad (1)$$

where W_{wet} or W_{dry} represents the weight of the membrane in the fully-swollen or dry state, respectively. The mass density of the dry membranes (ρ_p) has been measured experimentally and listed in Table 1, thus the total water volume fraction (ϕ_w) of a given membrane can be calculated by eq. (2) below and is listed in Table 1 as well.

$$\phi_w = \frac{\rho_p U}{\rho_w + \rho_p U} \qquad (2)$$

where ρ_w is the mass density of water. Thus the volume fraction of PSP blocks, $\phi_{PSP} = \frac{\frac{M_{PSP}}{\rho_{PSP}}}{\frac{M_{PSP}}{\rho_{PSP}}+\frac{M_{PAEK}}{\rho_{PAEK}}}(1-\phi_w)$, or PAEK blocks, $\phi_{PAEK} = 1-(\phi_w+\phi_{PSP})$, in the wet state has also been calculated and summarized in Table 1, where M_X and ρ_X (X = PSP or PAEK) are the molecular weight of X blocks in the polymer and the mass density of X, respectively. Note that ρ_{PSP} and ρ_{PAEK} are deduced from the molar ratio of the two blocks and ρ_p of dry membranes as 1.495 and 1.32 g/cm^3, respectively.

Since the ion exchange capacity (IEC) increases with the number of solvated PSP blocks, the proton conductivity of the two membranes is different accordingly. The proton conductivity of PSP_{14}-*b*-$PAEK_{14}$ and PSP_{28}-*b*-$PAEK_{14}$ membranes at 90% relative humidity and 30 ºC has been reported in the previous paper [1] and listed in Table 1. It was found that PSP_{28}-*b*-$PAEK_{14}$ membrane has higher proton conductivity than PSP_{14}-*b*-$PAEK_{14}$ membrane. In the following sections, we will elucidate this difference in terms of the structure.

II-2. Small-angle Neutron Scattering (SANS) measurement. SANS measurements were performed with KWS-2 at the neutron source Heinz Maier-Leibnitz (FRM II reactor) in Garching, Germany [35]. The incident neutron beam was monochromatized with a velocity selector to have the average wavelength (λ) of 5 Å with a wavelength resolution of $\Delta\lambda / \lambda$ = 20%. All of the measurements were done at 25 ± 0.5 °C. The scattering patterns were collected with a two-dimensional scintillation detector, and circularly averaged to obtain scattering intensity profiles as a function of q. The obtained scattering profiles were corrected

for the instrument background, detector sensitivity, and scattering from empty cell, and finally calibrated on the absolute scale (cm^{-1}) using a Plexiglas secondary standard. The scattering intensity profile of each water mixture of H_2O and D_2O was measured in a quartz cell with a thickness of ~ 0.5 mm, and used to estimate the incoherent scattering intensity for each water-swollen membrane with respect to its thickness and water-uptake. The estimated incoherent scattering intensity was subtracted from the absolute scattering intensity of each profile.

II-3 Hard-Sphere (HS) model analysis. We assume that the topology of the swollen membranes can be described by an almost random distribution of n particles in a homogeneous matrix. Let Δb be the contrast of the particle density with respect to the matrix density and v be the average volume of a single particle, then the observed scattering intensity, $I(q)$, is [36]

$$I(q) = (\Delta b)^2 n v^2 P(q) S(q) = K P(q) S(q) \qquad (3)$$

where $P(q)$ is the form factor of the particles, $S(q)$ is an approximate interference factor and K is a constant in terms of Δb, n and v. We assume that the number of the particles per volume is high that $S(q)$ must be considered despite the random arrangement of the particles. The contrast $\Delta b = b_p - b_m$ is defined by the difference between the scattering length density (SLD) of the particle phase, b_p, and that of the matrix phase, b_m. Thus, Δb is computable as long as the shape and composition of the particle phase and the matrix phase are well determined, and their SLDs are theoretically estimated below.

SLD of a molecule of i atoms is related to its molecular structure and may be readily calculated from the simple expression given by $b = \sum_i b_i \frac{dN_A}{M_w}$ where b_i is the scattering length of ith atom, d is the mass density of the scattering body, M_w is the molecular weight, and N_A is the Avogadoro constant [36].

Let us consider an ensemble of spheres with varying sizes that can be described by a

Gaussian size distribution:

$$P(q) = \int_0^\infty \left\{\frac{3}{(qr)^3}[\sin(qr) - qrcos(qr)]\right\}^2 \times \frac{1}{(2\pi)^{1/2}\sigma_R}\exp[\frac{-(r-R)^2}{2{\sigma_R}^2}]dr \qquad (4)$$

with R being the average radius, and σ_R being its standard deviation. Thus $v = \frac{4\pi R^3}{3}$. We consider Percus–Yevick expression to account for interparticle interference [37,38], then $S(q)$ is the interference factor, described for a random arrangement of spheres by the following expression

$$S(q, R, \phi) = \frac{1}{1+24\phi(\frac{F(A)}{A})} \qquad (5)$$

here $A = 2qR$ and ϕ is the hard sphere volume fraction. $F(A)$ is a trigonometric function of A and ϕ given by

$$F(A) = \frac{\alpha}{A^2}(sinA - AcosA) + \frac{\beta}{A^3}(2AsinA + (2 - A^2)cosA - 2) + \frac{\gamma}{A^5}(-A^4cosA +$$

$$4[(3A^2 - 6)cosA + (A^3 - 6A)sinA + 6]) \qquad (6)$$

where

$$\alpha = (1 + 2\phi)^2/(1 - \phi)^4$$

$$\beta = -6\phi\left(1 + \frac{\phi}{2}\right)^2/(1 - \phi)^4$$

$$\gamma = \frac{1}{2\phi}(1 + 2\phi)^2/(1 - \phi)^4 \qquad (7)$$

At $q = 0$, eq. (3) can be written as $I(0) = \Delta b^2 n v^2 P(0) S(0)$. Since $\phi = nv$, $P(0) = 1$ and $S(0) = 1/\alpha$, thus

$$I(0) = \Delta b^2 \phi v/\alpha \qquad (8)$$

Note that $I(0)$ on the left hand side (lhs) of eq. (8) can be experimentally extrapolated, and the right hand side (rhs) of eq. (8) can be theoretically calculated in terms of ϕ, v and α being determined by HS model. Therefore, the consistency of the lhs and rhs of eq. (8) enables us to verify the structure models, which will be discussed in conjunction with Figure 5 in section IV-2.

III. Results

III-1, Dry membranes and membranes equilibrated in D_2O. When a dry membrane is emerged into water, the hydrophilic blocks with sulfonic groups can absorb water and form hydrated regions, where the protons are able to transport, hence the proton conductivity is created. Thus in order to improve the proton transport efficiency of the membrane, the understanding of the swelling behavior and the morphology of the hydrated regions in the wet membrane is very crucial. In this section, we will report how the morphology of the membranes changes upon swelling.

Figure 2a presents SANS profiles for dry PSP_{14}-*b*-$PAEK_{14}$ membranes (profile 1, opened circles) and membranes equilibrated in D_2O (profile 2, opened squares) at room temperature, respectively. Both the shape and intensity of the profiles varied significantly before and after swelling, indicating a big change in the morphology upon swelling. In the dry state, $I(q)$ is weak and q-independent except for the upturn in the small-q range at $q < 0.01$ Å^{-1} and a small scattering maximum at $q = 0.22$ Å^{-1}. According to the scattering theory [36], $I(q)$ of the dry membranes is proportional to the square of the scattering contrast, which is the difference in the SLD between PSP and PAEK blocks. Hence the weak $I(q)$ reveals a low scattering contrast. We estimated the SLD of PSP (without taking solvated ionic groups into account) blocks and PAEK blocks theoretically being 2.84 and 2.37 ($\times 10^{10}$ cm^{-2}), respectively [39]. The small difference in SLD between the two blocks was confirmed, which is reasonable due to their similar molecular structures.

At $q < 0.01$ Å^{-1}, a clear upturn is observed and we notice that $I(q)$ vs q follows a power-law function at different q-ranges: at $q < 0.004$ Å^{-1}, a typical Porod law for the smooth interface is observed, *i.e.* $I(q) \sim q^{-4}$ [40], which is due to the scattering from the relatively smooth interface between ionomer-rich regions and ionomer-poor regions; At 0.004 Å$^{-1} < q < 0.01$ Å^{-1}, a power law shows $I(q) \sim q^{-2}$, seemingly indicating a lamellar structure, though no typical lamellar periodical peaks were observed at $q > 0.01$ Å^{-1}. The lower limit for the lamella thickness from $q_{L,min} = 0.004$ Å^{-1} gives a maximum d-spacing ($=2\pi/q_{L,min}$) about 157

nm. The possible lamellar signature will be further discussed in Section VI in conjunction with morphology models.

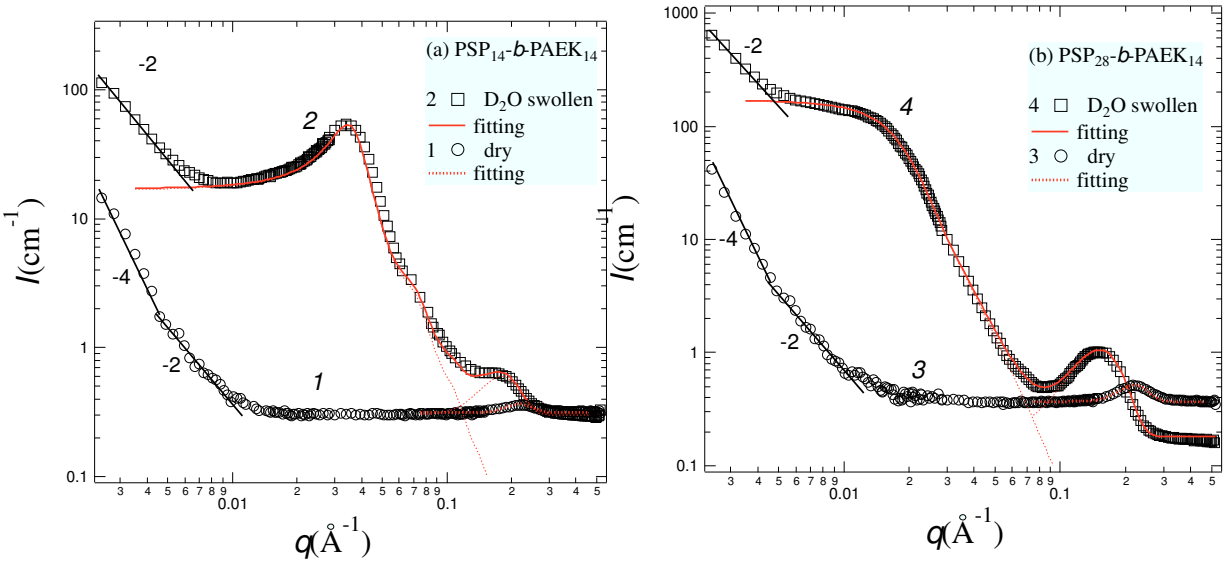

Figure 2

The small scattering maximum (ionomer peak) clearly shown in profile 1 at the peak position, $q_{m,ion}$ (= 0.22 Å^{-1}), reveals the mean distance between the sulfonic ionic clusters randomly distributed along the polymer chains to be $d \equiv 2\pi/q_{m,ion}$ = 28.5 Å. This value is very close to the recent reported data of 23 Å in sulfonated poly(ether ether ketone) (sPEEK) system with a similar sulfonation degree [41]. However, the direct SANS signal of the dry sample in ref. 41 was too low to give the structure signature. In the present study, the ionomer peak was clearly observed. This may be partially due to an increased scattering contrast induced by the multiblock chain structure, and partially due to the narrow distribution of ionic clusters. The distribution of the ionic clusters can be fitted well by Gaussian distribution function, where the scattering intensity around the ionomer peak at 0.08 Å^{-1} < q < 0.45 Å^{-1}, $I_{ion}(q)$, can be expressed by eq. (9) below

$$I_{ion}(q) = I_{m,ion}G(q) + I_{inc} \qquad (9)$$

where $I_{m,ion}$ is the iomomer peak height, $G(q)$ is Gaussian distribution function about the

ionomer peak at $q_{m,ion}$, given by $G(q) = \frac{1}{(2\pi)^{1/2}\sigma_q}\exp[-(q - q_{m,ion})^2/(2{\sigma_q}^2)]$, with σ_q being the standard deviation of $q_{m,ion}$, and I_{inc} is the incoherent scattering intensity, which can be determined by the average intensity of the flat part of the profile at q > 0.4 Å^{-1} in the high-q region. Eq. (9) is used to fit profile 1 and the best-fitted theoretical curve (dashed red line) is presented in the figure as well. The relative standard deviation, $\sigma_q/q_{m,ion}$, for the dry membrane was thus determined to be 0.136. The best fitted results of the iomomer peak for the membranes in both dry and wet (in the water mixture with different H_2O/D_2O ratios) states are listed in Table 2.

Note that profile 1 in Figure 2a for the dry membranes only exhibits one scattering maximum of the ionomer peak at high-q range, but no crystalline peaks appear in the middle-q range. Generally, PAEK polymers, oligomers and their derivatives are known to be semicrystalline polymers [42-44], therefore, similar to Nafion [45-47], the SANS spectra of these polymers with low sulfonation degree [41] usually exhibit two scattering maxima attributing to the ionomer and crystalline domains, respectively. However, the crystallinity index decreases with the increasing sulfonation degree. For instance, sPEEK membranes are reported to be amorphous when a sulfonation degree is over 50% [48]. The absence of crystalline maximum in profile 1 (and in profile 3 as well) supports the conclusion that $[PSP_x\text{-}b\text{-}PAEK_y]_n$ membranes in the present study are amorphous, which was also confirmed by differential scanning calorimetry (DSC) measurement. This possibly results from the high sulfonation degree and the sequence interruption by the multiblock structures.

Profile 2 of the fully D_2O-swollen PSP_{14}-*b*-$PAEK_{14}$ membranes is also shown in Figure 2a. We observe that: 1) $I(q)$ is much larger than that of profile 1 throughout the whole q range except for that at q > 0.3 Å^{-1}. Note that water has been absorbed saturatedly around hydrophilic PSP blocks with a total U value of 0.2 to form hydrated regions. The scattering contrast between the hydrated regions and hydrophobic regions is much enhanced because the

absorbed heavy water has a large SLD, which increases the average SLD of the hydrated regions effectively [39]. In the high-q range at $q > 0.3$ Å^{-1}, $I(q)$ was found to be q-independent and slightly lower than that of profile 1. Note that in this q range, $I(q)$ is mainly due to the incoherent scattering intensity, I_{inc}, hence it suggests a fact that I_{inc} of the D_2O-swollen membrane is lower than that of the dry membrane. Note that I_{inc} is simply proportional to the total number of hydrogen atoms in the volume irradiated by the incident neutron beam, therefore, the incorporation of D_2O in the scattering volume has no contribution to I_{inc}, however, the swelling effect by D_2O increases the distance between two neighbored hydrophilic blocks, and reduces the number density of hydrogen atoms covalently bonded on the blocks in a given scattering volume, consequently, I_{inc} decreases.

In addition to the change in $I(q)$ described in 1), we also observe the following changes in the shape of the profile 2 arising from the swelling effects: 2) ionomer peak at the high-q range is more obvious due to the enhanced scattering contrast with the incorporation of D_2O, and the peak position shifts towards low-q range from 0.22 to 0.18 Å^{-1}, indicating an increased mean distance to 34.9 Å upon swelling. $\sigma_q/q_{m,ion}$ of the wet membrane was determined to be 0.194 (see Table 2); 3) A strong scattering maximum in the middle-q region appears, which is due to the formation of the hydrated regions as a result of water induced microphase separation. The profile in this region can be fitted well by using HS-model. The best fit was obtained with R = 8.5 nm, σ_R/R = 0.247 and ϕ = 0.32 as shown in Table 2. The resultant best-fitted curves at the middle-q range and high-q range are shown by the dashed red lines separately in the figure, and their sum-up curve is also shown by the solid red line; 4) the upturn appears at $q < 0.007$ Å^{-1} and $I(q)$ vs q follows the power law function of $I(q) \sim q^{-2}$, indicating the possible lamellar structure conserved from the dry membranes. However, the upturn shifts to the low-q range and its intensity is much increased in comparison with that of the dry membranes, revealing that the lamellar d-spacing increases with the incorporated D_2O inside one lamella.

Figure 2b presents scattering profiles for PSP_{28}-*b*-$PAEK_{14}$ membranes measured in both dry (profile 3, opened circles) state and equilibrated in D_2O (profile 4, opened squares) at room temperature, respectively. All of the swelling effects from 1) to 4) mentioned above were found in PSP_{28}-*b*-$PAEK_{14}$ membranes as well, but much more enhanced: 1) $I(q)$ of profile 4 at $q < 0.3$ A^{-1} is much enhanced due to the increased contrast by the large water uptake up to 0.65. At $q > 0.3$ $Å^{-1}$, $I(q)$ was found to be much lower than profile 3 because I_{inc} is further decreased due to the larger D_2O swelling effect. 2) ionomer peak in profile 4 is also enhanced, and the peak position shifts to the left more from 0.22 to 0.15 $Å^{-1}$ (see Table 2), indicating a larger d of the wet membrane being 41.9 Å; 3) the broad scattering maximum original from the formation of the hydrated regions appears in the middle-q range. The values of R, σ_R/R and ϕ of the microdomains formed in wet PSP_{28}-*b*-$PAEK_{14}$ membranes were determined from the best fitting by HS model to be 145 Å, 0.245 and 0.07 as shown in Table 2, respectively. The best fitted curves at the middle-q range and high-q range, and their sum-up are shown in the figure by dashed and solid red lines, respectively; 4) the upturn at $q < 0.01$ $Å^{-1}$ is as same as that was observed in Figure 2a. The swelling behaviors for the two types of membranes are similar, indicating the morphologies of the two as-cast dry membranes are similar, where the sulfonic groups are distributed more or less homogeneously in the membranes.

III-2, Polymer-solvent contrast variation. In this section, contrast variation SANS measurements on the two membranes, which were equilibrated in the mixtures of normal water and deuterated water with different volume ratios, are performed. According to these results, we shall check the validity of the model analysis, which we have used to elucidate the swelling behavior of the membranes in section III-1, and will find the matching point where the scattering contrast is minimum.

III-2.1 Validity of HS model analysis. Since the structure of the membranes is believed to be invariant whether the solvent is normal or deuterated, a valid structural model should give the

same values of R, σ_R/R and ϕ when it is applied to fit the experimental data at all contrasts. Figures 3a and 3b show the scattering profiles of PSP_{14}-*b*-$PAEK_{14}$ and PSP_{28}-*b*-$PAEK_{14}$ membranes swollen in water mixtures of normal water and deuterated water with different volume ratios, respectively. All of the profiles at middle-q range can be well-fitted by HS model with the same values of R, σ_R/R and ϕ (see Table 2 and the fitting curves in sold lines in Figures 3a and 3b). It confirms the validity of the HS model analysis.

Note that HS model also works well to fit the scattering data of the partially swollen membranes, where the membranes were equilibrated at a given relative humidity (RH = 30%). Similar sphere size (peak position) and the size distribution but different volume fractions were obtained from the partially swollen samples in comparison with the fully swollen samples, which not only confirm the validity of the HS model analysis, but also clarify that the other model having periodicity such as lamellae or cylinders is not proper to describe the morphology of hydrated regions in the middle-q range, because in those models the peak position should have shifted with water content. The detailed model analysis of PSP_{14}-*b*-$PAEK_{14}$ and PSP_{28}-*b*-$PAEK_{14}$ membranes equilibrated at RH = 30% can be found in Ref [49] in conjunction with Figures 1a and 1b in Ref [49].

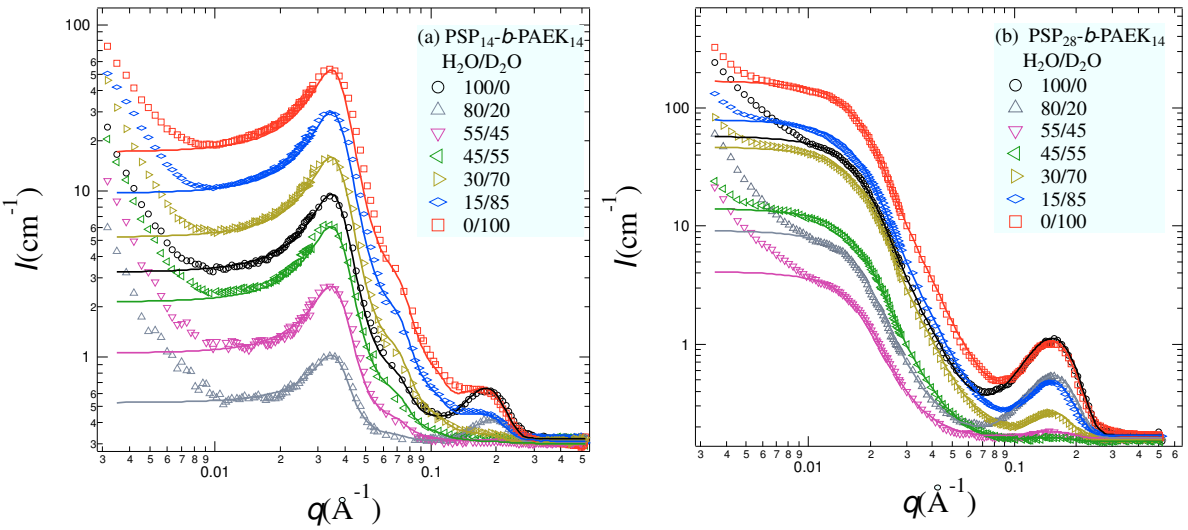

Figure 3

III-2.2 Matching points. The scattering maxima at the middle-q range ($I_{m,HM}$) and peak heights at high-q range ($I_{m,ion}$) are obtained for the profiles at all contrast, and they vary as a function of the volume fraction of deuterated water in the water mixture, f_{D2O}.

Figure 4a shows the plot of $I_{m,HM}$ versus f_{D2O} for both PSP_{14}-*b*-$PAEK_{14}$ and PSP_{28}-*b*-$PAEK_{14}$ membranes. Note that only a shoulder instead of a peak appears in the scattering profiles of the wet PSP_{28}-*b*-$PAEK_{14}$ membranes, therefore we plot the scattering intensity at q ~ 0.0098 $Å^{-1}$ as $I_{m,HM}$. The fraction of f_{D2O} at which a minimum $I_{m,HM}$ appears means the contrast matching point where the scattering contrast between the hydrated and hydrophobic domains is minimum. The volume fraction of deuterated water at the matching point, y_{HM}, was found to be of ~32% for PSP_{14}-*b*-$PAEK_{14}$ membranes and of ~35% for PSP_{28}-*b*-$PAEK_{14}$ membranes, respectively.

The evolution of $I_{m,ion}$ with f_{D2O} is presented in Figure 4b for both PSP_{14}-*b*-$PAEK_{14}$ and PSP_{28}-*b*-$PAEK_{14}$ membranes. The volume fraction of deuterated water at the matching point in the high-q range, y_{ion}, where $I_{m,ion}$ is minimum, was found to be the same for both membranes of ~50%. At y_{ion}, nearly no ionomer peak was observed, revealing that the SLD of hydrophilic PSP blocks, b_{PSP}, matches that of the water, $b_{w,ion}$. $b_{w,ion}$ can be estimated by the volume averaged SLD of D_2O and H_2O in the mixture, given by $b_{w,ion} = y_{ion}b_{D2O} + (1 - y_{ion})b_{H2O}$, where b_{D2O} = 6.34 × 10^{10} cm^{-2} and b_{H2O} = -0.56 × 10^{10} cm^{-2} are the SLD of D_2O and H_2O, respectively [34]. Thus b_{PSP} = 2.89 × 10^{10} cm^{-2} is estimated, and in good agreement with the value of 2.84 × 10^{10} cm^{-2} calculated from the chemical formula without taking solvated ionic groups into account as mentioned in section III-1 [39,42]. This result confirms the correctness of b_{PSP}.

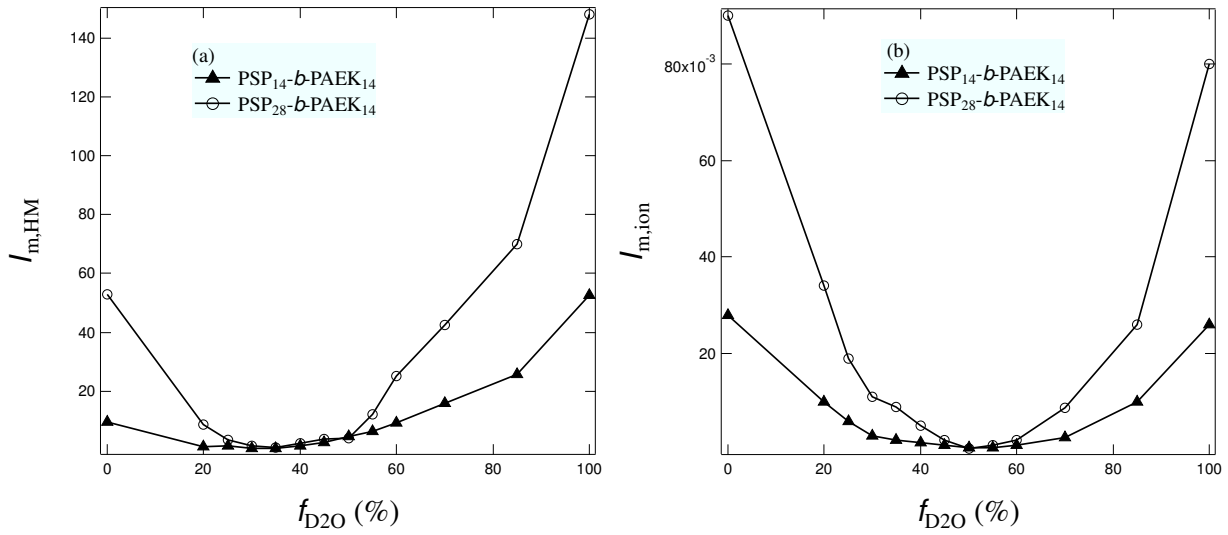

Figure 4

IV. Discussion

IV-1 Large length scale morphology at low-*q* rang. Although the polymer used in this study is evidenced to be amorphous, their natural tendency to crystallize may generate some polymer chain alignments that favor the formation of lamellar structures, as what has been reported by Gebel [41] that the lamellar structure seems intrinsic to sulfonated ether ketone polymers, though not a direct consequence of their semicrystalline nature. Since the current experimental temperature is far below the glass transition temperature of the polymer (~ 230 ^{o}C), the lamellar structure frame formed in the dry membranes is conserved in the swelling process. The incorporation of water in ionic clusters just creates new patterns (spheres) of hydrated regions within lamellae. Furthermore, the q^{-2} power law of the scattering intensity at low-q range has been observed for both dry (0.004 Å^{-1} < q < 0.01 Å^{-1}) and wet membranes (q < 0.004 Å^{-1}) in Figures 2a and 2b, which possibly indicates a lamellar spacing at a large length scale about 1500 Å (=2π/0.004) for the dry sample and larger than 1500 Å for the wet sample, respectively. Within a lamella, the morphology of hydrated regions in the wet membranes is proposed to be randomly distributed spheres as described by HM models in section III and illustrated in Figure 5.

IV-2 Interconnected hydrated regions. To judge the hydrated regions are interconnected or not, we first assume a perfect HS model that the spheres are isolated and the hydrated domains are composed of PSP blocks and water. Based upon this assumption, we think about two types of dispersions of the hydrated regions schematically shown in Figure 5a: hydrophilic spheres in the hydrophobic matrix; and Figure 5b: hydrophobic spheres in the hydrophilic matrix. In this section, we will discuss these two models separately.

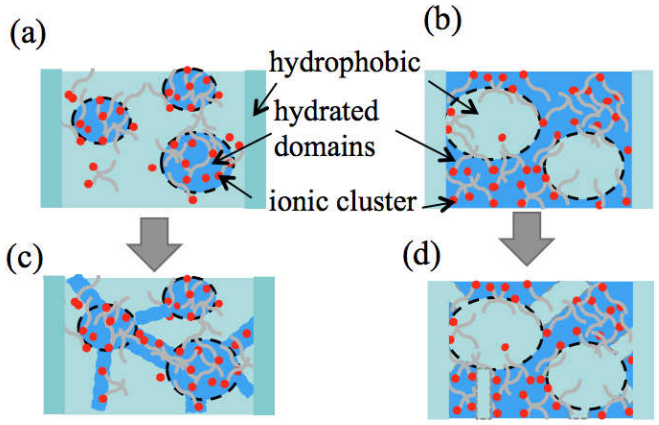

Figure 5

IV-2.1 Case of Figure 5a. In this case, the hydrated spheres are proposed to disperse in the hydrophobic matrix. Thus SLD of hydrated spheres, b_{sphere}, is given by the averaged SLD of all the components in the spheres as

$$b_{sphere} = \frac{b_{PSP}\phi_{PSP}^{in} + b_w\phi_w^{in}}{\phi_{PSP}^{in} + \phi_w^{in}} = \frac{b_{PSP}\phi_{PSP}^{in} + b_w\phi_w^{in}}{\phi} \qquad (10)$$

where b_x means the SLD of x (x= PSP or w, being PSP blocks and water mixture, respectively). ϕ_x^{in} means the volume fraction of x in the hydrated sphere regions, and ϕ is the volume fraction of spheres estimated by HS model. Thus $\phi_{PSP}^{in} + \phi_w^{in} = \phi$.

The hydrophobic matrix is assumed to be made of PAEK chains mainly, thus the SLD of the matrix, b_{matrix}, can be roughly calculated by the SLD of PAEK blocks, b_{PAEK}, as follows

$$b_{matrix} = b_{PAEK} \qquad (11)$$

Thus, b_{matrix} is estimated to be 2.37×10^{10} cm^{-2}.

We first consider PSP$_{14}$-*b*-PAEK$_{14}$ membranes. At the matching point, the contrast

between hydrated spheres and matrix disappears and gives $b_{sphere} = b_{matrix}$. b_w in eq. (10) can be calculated as a function of f_{D2O} as below

$$b_w = b_{D2O} f_{D2O} + b_{H2o}(1 - f_{D2O}) \qquad (12)$$

At the matching point, $f_{D2O} = y_{HM} \sim 32\%$. Bring y_{HM} back to Eqs (10) ~ (12), we have ϕ_w^{in} = 0.132 and ϕ_{PSP}^{in} = 0.188, and these results are listed in Table 3. The total volume fraction of water or PSP, ϕ_x (x = w or PSP) shown in Table 1 was found to be larger than ϕ_x^{in}. The deviation between ϕ_x^{in} and ϕ_x, designated as ϕ_x^{out}, is proposed to be x distributed in the matrix, which forms hydrated channels to interconnect the hydrated spheres and offer the important proton conductivity. The scattering by these channels is believed to be much smaller than that from the dominant sphere regions. ϕ_x^{out} for PSP_{14}-*b*-$PAEK_{14}$ membranes is thus given as follows: $\phi_w^{out} = \phi_w - \phi_w^{in} = 0.068$ and $\phi_{PSP}^{out} = \phi_{PSP} - \phi_{PSP}^{in} = 0.279$. These results are also listed in Table 3.

The same calculations were also made for PSP_{28}-*b*-$PAEK_{14}$ membranes with respect to $y_{HM} \sim 35\%$ at the matching point. The resultant ϕ_w^{in} is 0.026 and ϕ_{PSP}^{in} is 0.044, both values are surprisingly smaller than ϕ_x^{out} values of water and PSP blocks being ϕ_w^{out} = 0.434 and ϕ_{PSP}^{out} = 0.286. This result forces us to think about the other possibility of the structure: hydrophobic PAEK spheres disperse in the hydrophilic matrix. We will discuss this possibility in the following case of Figure 5b.

Note that considering the existence of ϕ_x^{out}, the model shown in Figure 5a should be corrected to the one shown in Figure 5c, where the interconnected hydrated channels can be taken into account as a part of the matrix.

IV-2.2 Case of Figure 5b. In this section, an inverse structure of the model in Figure 5a is proposed, which is characterized by the dispersion of hydrophobic spheres in a hydrophilic matrix. The SLD of the hydrophobic sphere regions, b_{sphere}, and that of the hydrated matrix, b_{matrix}, thus are given by

$$b_{sphere} = b_{PAEK} \qquad (13)$$

$$b_{matrix} = \frac{b_{PSP}\phi_{PSP} + b_w\phi_w}{\phi_{PSP} + \phi_w} \qquad (14)$$

At the matching point of y_{HM}, eq (14) gives $b_{matrix} \sim 2.39 \times 10^{10}$ cm^{-2} for PSP$_{14}$-*b*-PAEK$_{14}$ membranes and 2.34×10^{10} cm^{-2} for PSP$_{28}$-*b*-PAEK$_{14}$ membranes, respectively. Both values are in good agreement with the theoretical value of $b_{PAEK} = 2.37 \times 10^{10}$ cm^{-2} in eq. (13). Hence, at y_{HM} the matching between hydrophobic PAEK spheres and hydrated matrix reasonably occurs. This result confirms not only the correctness of b_{PAEK}, but also the possibility that membranes might have an inverse matrix.

Note that though the hydrophobic spheres are assumed to be made of PAEK blocks, we found $\phi < \phi_{PAEK}$ for both samples, thus the deviation between ϕ and ϕ_{PAEK} is defined as ϕ_{PAEK}^{out} (= ϕ_{PAEK} - ϕ) being the volume fraction of PAEK distributed out of the sphere regions, in the other word, it is proposed to be the bridges to connect the hydrophobic PAEK spheres. Thus according to the model in Figure 5b, the determined ϕ_{PAEK}^{out} is 0.133 for PSP$_{14}$-*b*-PAEK$_{14}$ membranes and 0.14 for PSP$_{28}$-*b*-PAEK$_{14}$ membranes, respectively. All these results are summarized in Table 3. Note that ϕ_{PAEK}^{out} is larger than ϕ in the case of PSP$_{28}$-*b*-PAEK$_{14}$ membranes, which can be understood if we take the ionomer-poor lamellae into account. Considering the existence of ϕ_{PAEK}^{out}, the model shown in Figure 5b has been corrected to the one shown in Figure 5d, where the PAEK bridges or interconnections are treated as a part of the matrix.

It should be also noted that similar to Nafion, both PSP$_{14}$-*b*-PAKE$_{14}$ and PSP$_{28}$-*b*-PAKE$_{14}$ show no melting endotherm upon the melting of frozen absorbed water via DSC measurement, indicating very loosely bound water under the current swollen sample conditions [50], which makes the quantitative determination of the fraction of bound water difficult. However, according to our previous study on cellulose membrane samples, the bound water can be roughly estimated by the weight difference between the naturally dried sample (*i.e.*, dried in air) and the completely dried sample by vacuum drying [51]. According to this method, the

bound water uptakes of PSP_{14}-*b*-$PAKE_{14}$ and PSP_{28}-*b*-$PAKE_{14}$ membranes are roughly estimated to be 3.0% and 4.6%, respectively. Then the remains of the water uptake of each sample are expected to be free water.

IV-3 Amphiphilicity of the matrix at middle-*q* range. The discussion in section IV-2 above confirms that the hydrated regions are interconnected, however, the amphiphilicity of the matrix might be either hydrophobic (shown in Figure 5c) or hydrophilic (shown in Figure 5d). In this section, we shall quantitatively judge the amphihilicity of the matrix in terms of contrast variation results.

Note that the expression of Δb (= $b_{\text{sphere}} - b_{\text{matrix}}$) in eq. (8) depends on the amphiphilicity of the spheres and matrix, hence the consistency of the lhs and rhs of eq. (8) enables us to verify the structure models. The cases of PSP_{14}-*b*-$PAEK_{14}$ and PSP_{28}-*b*-$PAEK_{14}$ membranes will be separately discussed as below.

IV-3.1 Case of PSP_{14}-*b*-$PAEK_{14}$. We will first consider PSP_{14}-*b*-$PAEK_{14}$ membranes in terms of the model in Figure 5c. Δb is given by

$$\Delta b = \frac{b_{PSP}\phi_{PSP}^{in} + b_w\phi_w^{in}}{\phi} - \frac{b_{PSP}\phi_{PSP}^{out} + b_w\phi_w^{out} + b_{PAEK}\phi_{PAEK}}{1-\phi} \qquad (15)$$

All of the parameters in eq. (15) have been listed in Table 3, except b_w, which depends on f_{D2O} and is given by eq. (12). Thus rhs of eq. (8) can be calculated as a function of f_{D2O}. $I(0)$ in eq. (8) can be estimated by extrapolating the best-fitted lines to q = 0 for all contrasts shown in Figure 3a. We plot the resultant $I(0)$ and rhs of eq. (8) for PSP_{14}-*b*-$PAEK_{14}$ membranes in Figure 6a, and a good consistency between $I(0)$ and rhs of eq. (8) is obtained with a linear relationship having a slope of 1.04 $\pm$ 0.03.

On the other hand, if one considers the model shown in Figure 5d. Δb is written by

$$\Delta b = b_{PAEK} - \frac{b_{PSP}\phi_{PSP} + b_w\phi_w + b_{PAEK}\phi_{PAEK}^{out}}{1-\phi} \qquad (16)$$

Similarly, all of the parameters in eq. (16), except b_w, are known as listed in Table 3. Thus rhs of eq. (8) can also be calculated as a function of f_{D2O}. The plot of $I(0)$ versus rhs of eq. (8) was

shown in Figure 6b, and the linear fitting gives a slope of 1.21 ± 0.02.

Compared to the model shown in Figure 5d, the model in Figure 5c works better for PSP_{14}-*b*-$PAEK_{14}$ membranes. Thus, the morphology of PSP_{14}-*b*-$PAEK_{14}$ membranes is characterized by a structure of interconnected hydrated spheres, embedded in the hydrophobic matrix. Note that the deviation between Figures 6a and 6b is not profound, indicating that the size and distribution of hydrated regions and hydrophobic regions are similar in PSP_{14}-*b*-$PAEK_{14}$ membranes.

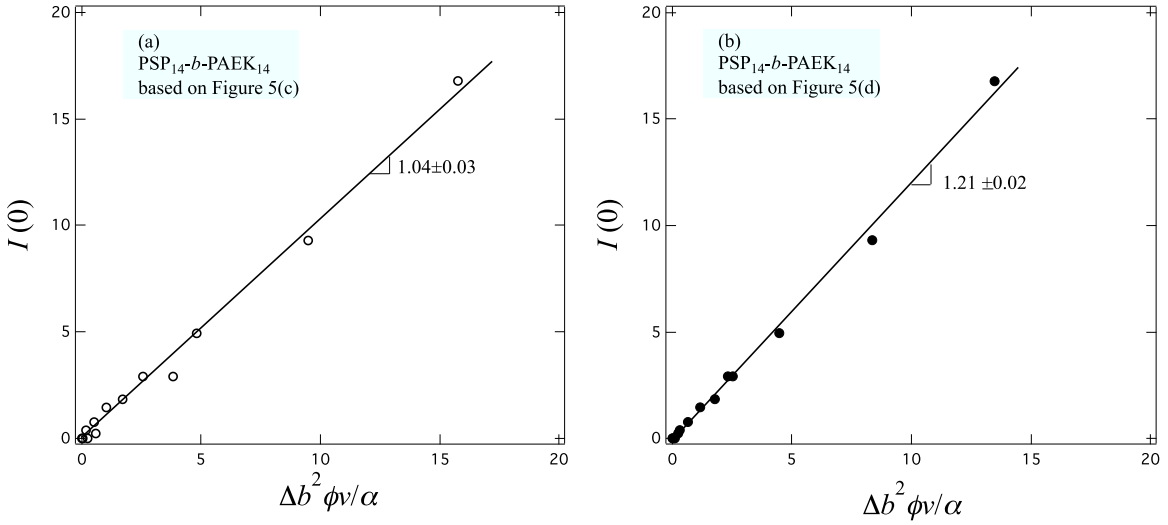

Figure 6

IV-3.2 Case of PSP_{28}-*b*-$PAEK_{14}$. In this section, we will consider the morphology of PSP_{28}-*b*-$PAEK_{14}$ membranes in terms of models shown in Figures 5c and 5d. Firstly, the velidity of the model in Figure 5c was checked by eq. (8). Δb can be calculated by eq. (15) and thus the rhs of eq. (8) can be deduced as a function of f_{D2O}. The plot of $I(0)$ versus rhs of eq. (8) is shown in Figure 7a, and the linear fitting shows a slope of 9.0 ± 0.4, indicating a very poor consistency, thus the model of Figure 5c was ruled out to describe the morphology of PSP_{28}-*b*-$PAEK_{14}$ membranes.

Next, we consider the model shown in Figure 5d. Δb can be given by eq. (16) and again the rhs of eq. (8) can be calcualted for all contrasts. The plot of $I(0)$ vs rhs of eq. (8) is shown in Figure 7b, and the linear fitting shows a slope of 0.81 $\pm$ 0.03, indicating a fairly good consistency between the two datasets. Therefore, the morphology of PSP_{28}-*b*-$PAEK_{14}$ membranes can be described well by the structure model shown in Figure 5d, where interconnected hydrophobic spheres are floating in the hydrated matrix.

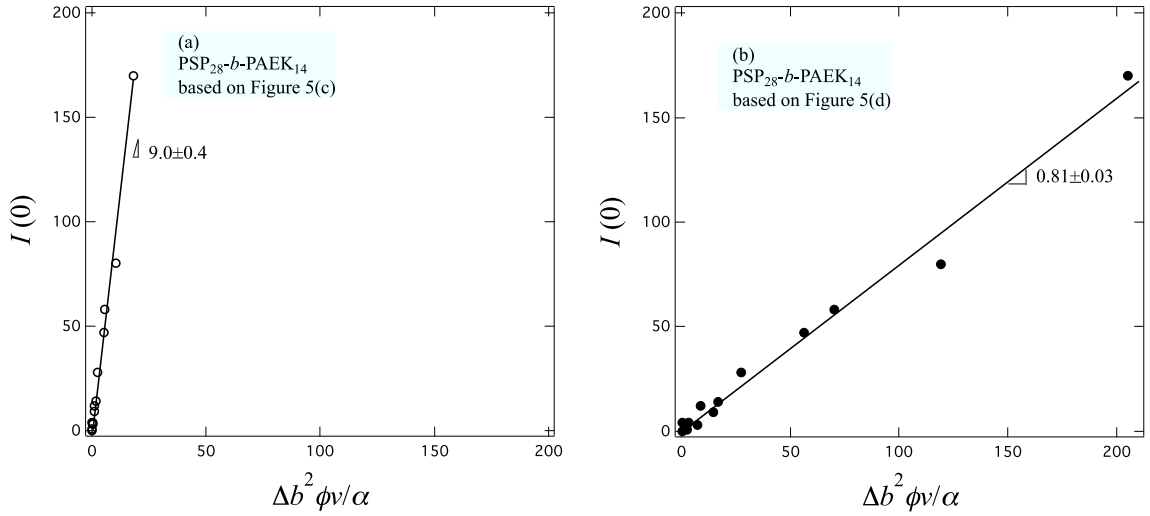

Figure 7

IV-4 Interplay between the morphology and property for PEMs. Let us next consider the interplay between the morphology and the property of the membranes. According to the discussions in section IV-2&3, the common characteristic structure of both PSP_{28}-*b*-$PAKE_{14}$ and PSP_{14}-*b*-$PAKE_{14}$ membranes is the existence of the interconnected hydrated regions, which is believed to play a key role to improve the proton conductivity of the membrane. In Table 1, the characterizations of IEC, water uptake and proton conductivity of each membrane were summarized. It can be found that PSP_{28}-*b*-$PAKE_{14}$ membrane exhibits relatively high IEC value (1.8 mmol/g) in comparison with that of PSP_{14}-*b*-$PAKE_{14}$ membrane (1.15 mmol/g) and the reported value of the benchmark: Nafion membrane (0.91 mmol/g) [52], revealing a larger density of acidic sulfonic groups in PSP_{28}-*b*-$PAKE_{14}$ sample. This result is consistent with the SANS analysis in the sections above, which shows that PSP_{28}-*b*-$PAKE_{14}$

membrane has more pronounced hydrophilic/hydrophobic microphase separation than PSP_{14}-*b*-$PAKE_{14}$ membrane evidenced by the larger hydrated regions as a matrix and the larger segregation power predicted by the more acidic sulfonic groups. On one hand, this leads to the high ion diffusion and water transport; on the other hand, the large and hydrated matrix might result to relatively poor mechanical properties.

V. Conclusion

In summary, we have employed contrast variation small angle neutron scattering method to investigate the structure of two synthesized hydrocarbon polymer electrolyte membranes composed of multiblock copolymers, poly(sulphonate phenylene)-*b*-poly(arylene ether ketone) with different block ratios. The scattering intensity upturn with q^{-2} power law at low-q range indicates a possible lamellar structure at the large length scale due to the semicrystalline nature of the polymers. Hard-Sphere model with Percus-Yervick interference approximation is able to fit the SANS data nicely in the middle-q range and describes the structure rationally over all contrasts. On the basis of HS model, we propose that hydrated sphere regions interconnected by hydrated channels are formed in both membranes, within which ionic clusters are randomly distributed. The morphology of the water swollen membranes depends on the ratio of hydrophilic blocks to hydrophobic blocks: PSP_{14}-*b*-$PAEK_{14}$ membrane which has less ionic groups is characterized by a network structure of interconnected hydrated spheres accompanied by a similar-sized interconnected PAEK hydrophobic regions as schematically shown in Figure 5c; while PSP_{28}-*b*-$PAEK_{14}$ membrane which has more ionic groups is characterized by the interconnected PAEK hydrophobic polymer spheres floating in the interconnected hydrated matrix, as schematically shown in Figure 5d. The interconnected hydrated regions are responsible for the desired property of PEMs, where high proton conductivity is expected through the membranes.

References and Notes.

[1] M. Yoshida, Y. Zhao, M. Yoshizawa-Fujita, A. Ohira, Y. Takeoka, S. Koizumi, and M. Rikukawa, PFG-NMR and SANS studies in cation exchange membranes based on sulfonated polyphenylene multiblock copolymers, ECS Trans. 50 (2013), 1045-1053.

[2] W. Vielstich, A. Lamm, H. Gasteiger, Handbook of fuel cells: fundamentals, technology, applications, John Wiley, 2004.

[3] S.G. Chalk, J.F. Miller, F.W. Wagner, Challenges for fuel cells in transport applications, J. Power Sources, 86 (2000), 40-51.

[4] G. Cacciola, V. Antonucci, S. Freni, Technology up date and new strategies on fuel cells, J. Power Sources, 100 (2001), 67-79.

[5] P. Costamagna, S. Srinivasan, Quantum jumps in the PEMFC science and technology from the 1960s to the year 2000: Part II. engineering, technology development and application aspects, J. Power Sources, 102 (2001), 253-269.

[6] A.F. Ghenciu, Review of fuel processing catalysts for hydrogen production in PEM fuel cell systems, Curr Opin Solid State Mater Sci., 6 (2002), 389-399.

[7] S. Gamburzev, A.J. Appleby, Recent progress in performance improvement of the proton exchange membrane fuel cell (PEMFC), J. Power Sources, 107 (2002), 5-12.

[8] V. Mehta, J.S. Cooper, Review and analysis of PEM fuel cell design and manufacturing, J. Power Sources, 114 (2003), 32-53.

[9] H.A. Gasteiger, J.E. Panels, S.G. Yan, Dependence of PEM fuel cell performance on catalyst loading, J. Power Sources, 127 (2004), 162-171.

[10] M.Z. Jacobson, W.G. Colella, D.M. Golden, Cleaning the air and improving health with hydrogen fuel-cell vehicles, Science, 308 (2005), 1901-1905.

[11] J.H. Wee, Applications of proton exchange membrane fuel cell systems, Renewable & Sustainable Energy Reviews, 11 (2007), 1720-1738.

[12] Q. Li, R. He, J.O. Jensen, N.J. Bjerrum, Approaches and recent development of polymer

electrolyte membranes for fuel cells operating above 100 °C, Chem. Mater., 15 (2003), 4896-4915.

[13] M.A. Hickner, H. Ghassemi, Y.S. Kim, B.R. Einsla, J.E. Mcgrath, Alternative polymer systems for proton exchange membranes (PEMs), Chem. Rev., 104 (2004), 4587-4612.

[14] J.S. Lee, N.D. Quan, J.M. Hwang, S.D. Lee, H. Kim, H. Lee, H.S. Kim, Polymer electrolyte membranes for fuel cells, J. Ind. Eng. Chem., 12 (2006), 175-183.

[15] S. Schlick, Ionomer: Characterization, theory and applications, CRC Press, Boca Raton, FL, 1996.

[16] K.A. Mauritz, R.B. Moore, State of understanding of Nafion, Chem. Rev., 104 (2004), 4535-4585.

[17] S. Zhong, C. Liu, H. Na, J. Membr. Sci., 326 (2009), 400-407.

[18] D. X. Luu, E.B. Cho, O. H. Han, D.J. Kim, SAXS and NMR analysis for the cast solvent effect on sPEEK membrane properties, J. Phys. Chem. B, 113 (2009), 10072-10076.

[19] E. A. Weiber, S. Takamuku, P. Jannasch, Macromolecules, 46 (2013), 3476-3485.

[20] J. Pang, S. Feng, Y. Yu, H. Zhang, Z. Jiang, Polym. Chem., 5 (2014), 1477-1486.

[21] Y. Yin, Q. Du, Y. Qin, Y. Zhou, K. Okamoto, J. Membr. Sci. 367 (2011), 211-219.

[22] X. Zhang, L. Sheng, T. Hayakawa, M. Ueda, T. Higashihara, J. Mater. Chem. A., 1 (2013) 11389-11396.

[23] F. Ng, D. J. Jones, J. Roziere, B. Bauer, M. Schuster, M. Jeske J. Membr. Sci., 362 (2010), 184-191.

[24] Q. Luo, H. Zhang, J. Chen, D. You, C. Sun, Y. Zhang, Preparation and characterization of Nafion/SPEEK layered composite membrane and its application in vanadium redox flow battery, Journal of membrane science, 325 (2008), 553-558.

[25] S. V. Sambasivarao, Y. Liu, J. L. Horan, S. Seifert, A. M. Herring, C. M. Maupin, Enhancing Proton Transport and Membrane Lifetimes in Perfluorosulfonic Acid Proton Exchange Membranes: A Combined Computational and Experimental Evaluation of the

Structure and Morphology Changes Due to $H_3PW_{12}O_{40}$ Doping, J. Phys. Chem. C 118 (2014), 20193-20202.

[26] T.D. Gierke, G.E. Munn, F.C. Wilson, The morphology in nafion perfluorinated membrane products, as determined by wide- and small-angle x-ray studies, J. Polym. Sci., Polym. Phys. Ed., 19 (1981), 1687-1704.

[27] M. Fujimura, T. Hashimoto, H. Kawai, Small-angle x-ray scattering study of perfluorinated ionomer membranes. 2. Models for ionic scattering maximum, Macromolecules, 15 (1982), 136-144.

[28] B. Loppinet, G. Gebel, C.E. Williams, Small-Angle scattering study of perfluorosulfonated ionomer solutions, J. Phys. Chem. B, 101 (1997), 1884-1892.

[29] G. Gebel, Structural evolution of water swollen perfluorosulfonated ionomers from dry membrane to solution, Polymer, 41 (2000), 5829-5838.

[30] A.L. Rollet, O. Diat, G. Gebel, A New Insight into Nafion Structure, J. Phys. Chem. B, 106 (2002), 3033-3036.

[31] G. Gebel, O. Diat, S. Escribano, R. Mosdale, Water profile determination in a running PEMFC by small-angle neutron scattering, J. Power Sources, 179 (2008), 132-139.

[32] K. Schmidt-Rohr, Q. Chen, Parallel cylindrical water nanochannels in Nafion fuel-cell membranes, Nat. Mater., 7 (2008), 75-83.

[33] H. Iwase, S. Koizumi, H. Iikura, M. Matsubayashi, D. Yamaguchi, Y. Maekawa, T. Hashimoto, A combined method of small-angle neutron scattering and neutron radiography to visualize water in an operating fuel cell over a wide length scale from nano to millimeter, Nucl Instrum. Methods A, 605 (2009), 95-98.

[34] I. Tonozuka, M. Yoshida, K. Kaneko, Y. Takeoka, M. Rikukawa, Considerations of polymerization method and molecular weight for proton-conducting poly(p-phenylene) derivatives, Polymer, 52 (2011), 6020-6028.

[35] A. Radulescu, V. Pipich, H. Frielinghaus, M.S. Appavou, KWS-2, the high intensity /

wide Q-range small-angle neutron diffractometer for soft-matter and biology at FRM II, Journal of Physics: Conference Series, 351 (2012), 012026.

[36] R.J. Roe, Methods of X-ray abd Neutron scattering in polymer science, Oxford Uni. Press, New York, 2000.

[37] J.K. Percus, G.J. Yevich, Analysis of classical statistical mechanics by means of collective coordinates, Phys. Rev., 110 (1958), 1-13.

[38] D.J. Kinning, E.L. Thomas, Hard-sphere interactions between spherical domains in diblock copolymers, Macromolecules, 17 (1984), 1712-1718.

[39] Similarly, SLD of D_2O and H_2O are theoretically calculated to be 6.34 and -0.56 ($\times 10^{10}$ cm^{-2}), respectively, the values of which will be used in the following sections to discuss the matching point.

[40] G. Porod, Die Rontgenkleinwinkelstrenung von dichtgepackten kolloiden Systemen, Kolloid Zeit, 124 (1951), 83.

[41] G. Gebel, Structure of membranes for fuel cells: SANS and SAXS analyses of sulfonated PEEK membranes and solutions, Macromolecules, 46 (2013), 6057-6066.

[42] M. Reitman, D. Jaekel, R. Siskey, S.M. Kurtz, Morphology and crystalline architecture of polyaryletherketones, in: S.M. Kurtz (Eds.), PEEK Biomaterials Handbook, Elsevier Press, New York, 2012, pp 49-60.

[43] T.W. Giants, Crystallinity and dielectric properties of PEEK, poly(ether ether ketone), IEEE Trans. Dielectr. Insul., 1 (1994), 991-999.

[44] O. Dupont, A.M. Joneas, B. Nysten, R. Legras, P. Adriaensens, J. Gelan, PEEK oligomers as physical model compounds for the polymer. 4. Lamellar microstructure and chain dynamics, Macromolecules, 33 (2000), 562-568.

[45] G. Gebel, P. Aldebert, M. Pineri, Swelling study of perfluorosulphonated ionomer membranes, Polymer, 34 (1993), 333-339.

[46] M. Fijimura, T. Hashimoto, H. Kawai, Small-angle x-ray scattering study of

perfluorinated ionomer membranes. 1. Origin of two scattering maxima, Macromolecules, 14 (1981), 1309-1315.

[47] G. Gebel, O. Diat, Neutron and X-ray scattering: suitable tools for studying ionomer membranes, Fuel Cells, 5 (2005), 261-276.

[48] V. Di Noto, M. Piga, G.A. Giffin, G. Pace, Broadband electric spectroscopy of proton conducting SPEEK membranes, J. Membr. Sci., 390-391 (2012), 58-67.

[49] Y. Zhao, M. Yoshida, S. Koizumi, M. Rikukawa, N. Szekely, A. Radulescu, D. Richter, Elucidation of the morphology of the hydrocarbon multi-block copolymer electrolyte membranes for proton exchange fuel cells, Data in Brief, submitted.

[50] A. I. Sodeye, T. Huang, S. P. Gido, J. W. Mays, Polymer electrolyte membranes from fluorinated polyisoprene-block-sulfonated polystyrene: structure evolution with hydration and heating, Polymer, 52 (2011), 3201-3208.

[51] Y. Zhao, S. Koizumi, D. Yamaguchi, T. Kondo, Hierarchical amorphous structure in microbial cellulose: what happens during the drying process, Eur. Phys. J. E., 37 (2014), 129.

[52] K. A. Mauritz, R. B. Moore, State of understanding of Nafion, Chemical Reviews, 104 (2004), 4535-4586.

Figure caption

Figure 1 Molecular structure of the multiple block copolymer $[PSP_x\text{-}b\text{-}PAEK_y]_n$ used in this study, where the subscript x and y refer to the repeating unit number of hydrophilic PSP blocks and hydrophobic PAEK blocks, respectively. n means the repeating number of the diblock segment unit.

Figure 2 Part (a): SANS profiles measured for dry (circles) and fully D_2O swollen (squares) PSP_{14}-*b*-$PAEK_{14}$ membranes at room temperature. The best-fitted curve at high-q range based on eq. (9) for the dry membrane is shown in the figure by the red dashed line. The best-fitted theoretical curve ranging from the middle-q region based on HS model (R = 85 Å, σ_R/R = 0.247 and ϕ = 0.32) to the high-q region based on eq. (9) for the swollen membrane is also shown in the figure by a red solid line. Part (b): SANS profiles measured for dry (circles) and fully D_2O swollen (squares) PSP_{28}-*b*-$PAEK_{14}$ membranes at room temperature. The best-fitted curve at high-q range based on eq. (9) for the dry membrane is shown in the figure by red dashed line. The best-fitted theoretical curve ranging from the middle-q region based on HS model (R = 145 Å, σ_R/R = 0.245 and ϕ = 0.07) to the high-q region based on eq. (9) for the swollen membrane is also shown in the figure by a red solid line.

Figure 3 Part (a): Contrast variations of the SANS profiles (symbols) obtained from PSP_{14}-*b*-$PAEK_{14}$ membranes swollen in water mixture at f_{D2O} = 100%, 85%, 70%, 55%, 45%, 20%, and 0%, respectively. The best-fitted theoretical profiles (solid line) based on the HS model analysis with the same R = 85 Å, σ_R/R = 0.247 and ϕ = 0.32 are also shown in the figure. Part (b): Contrast variations of the SANS profiles (symbols) obtained from PSP_{28}-*b*-$PAEK_{14}$ membranes swollen in water mixture at f_{D2O} = 100%, 85%, 70%, 55%, 45%, 20%, and 0%, respectively. The best-fitted theoretical profiles (solid line) based on the HS model analysis with the

same R = 145 Å, σ_R/R = 0.245 and ϕ = 0.07 are also shown in the figure.

Figure 4 Part (a): f_{D2O} dependence of the scattering maximum observed in the middle-q region ($I_{m,HM}$) for PSP_{14}-b-$PAEK_{14}$ and PSP_{28}-b-$PAEK_{14}$ membranes swollen in water mixtures of H_2O and D_2O with different volume ratios. $I_{m,HM}$ for PSP_{28}-b-$PAEK_{14}$ membranes is practically selected to be the intensity at q = 0.0098 $Å^{-1}$. Part (b): f_{D2O} dependence of the height of the peak observed at the high-q region ($I_{m,ion}$) obtained by eq. (9) for PSP_{14}-b-$PAEK_{14}$ and PSP_{28}-b-$PAEK_{14}$ membranes swollen in water mixtures of H_2O and D_2O with different volume ratios.

Figure 5 Possible models to elucidate the morphologies: (a) hydrated spheres (in blue) in a hydrophobic matrix (in gray); (b) hydrophobic spheres (in gray) in a hydrated matrix (in blue); (c) interconnected hydrated spheres in a hydrophobic matrix; (d) interconnected hydrophobic spheres in a hydrated matrix.

Figure 6 Plot of $I(0)$ as a function of $\Delta b^2 \phi v/\alpha$ for PSP_{14}-b-$PAEK_{14}$ membranes according to Part (a): Figure 5(c); Part (b): Figure 5(d).

Figure 7 Plot of $I(0)$ as a function of $\Delta b^2 \phi v/\alpha$ for PSP_{28}-b-$PAEK_{14}$ membranes according to Part (a): Figure 5(c); Part (b): Figure 5(d).

Table 1 Characteristics of the two membranes used in this study.

	PSP_{14}-*b*-$PAEK_{14}$	PSP_{28}-*b*-$PAEK_{14}$
M_n ($\times 10^{-3}$)[a]	22.0	58.0
M_w/M_n	3.2	2.2
n[b]	2	3.5
d_p (g/cm^3)[c]	1.39	1.43
Ion Exchange Capacity (IEC) (meq/g)[d]	1.15	1.8
Proton conductivity at 30 ºC (mS/cm)	15.4	16.5
U[e]	0.20	0.65
ϕ_w[f]	0.20	0.46
ϕ_{PSP}[g]	0.347	0.33
ϕ_{PAEK}[g]	0.453	0.21

a: Determined by SEC using Dimethylformamide (DMF) as an eluent.

b: Averaged degree of polymerization of each sample estimated from its M_n.

c: Averaged mass density calculated from the weight and volume of the given dry membrane.

d: Determined by back titration.

e: Measured in D_2O at 25 ºC.

f: Volume fraction of water incorporated in the wet membranes calculated from eq. (2).

g: Volume fractions of PSP blocks and PAEK blocks incorporated in the wet membranes, on the basis of the mass density of which being 1.495 or 1.32 g/cm^3, deduced from d_p of the two dry membranes.

Table 2 Parameters used to fit SANS results for PSP_{14}-*b*-$PAEK_{14}$ and PSP_{28}-*b*-$PAEK_{14}$ membranes in the dry and fully-swollen states by eqs. (3) & (9)

PSP_{14}-*b*-$PAEK_{14}$	middle-*q* range (HS model)				high-*q* range (ionomer peak)		
	ϕ	R (Å)	σ_R/R	K	$I_{m,ion}$	$q_{m,ion}$ (Å^{-1})	$\sigma_q/q_{m,ion}$
dry	-	-	-	-	0.004	0.22	0.136
fully-swollen with f_{D2O} (%)							
0				36.5	0.028		
20				2.84	0.01		
45				9.44	0.001		
55	0.32	85	0.247	23.0	0.0005	0.18	0.194
70				62.0	0.0025		
85				117.0	0.01		
100				211.3	0.026		

PSP_{28}-*b*-$PAEK_{14}$	middle-*q* range (HS model)				high-*q* range (ionomer peak)		
	ϕ	R (Å)	σ_R/R	K	$I_{m,ion}$	q_m (Å^{-1})	σ_q/q_m
dry	-	-	-	-	0.004	0.22	0.136
fully-swollen with f_{D2O} (%)							
0				100.8	0.09		
20				15.8	0.034		
45				6.95	0.002		
55	0.07	145	0.245	24.3	0.001	0.152	0.243
70				81.7	0.0088		
85				139.0	0.026		
100				295.3	0.08		

Table 3 Parameters deduced from contrast variation SANS results on the basis of the models shown in Figures 5c and 5d.

Sample	Models					
	Figure 5c				Figure 5d	
	ϕ_w^{in}	ϕ_w^{out}	ϕ_{PSP}^{in}	ϕ_{PSP}^{out}	ϕ_{PAEK}^{in}	ϕ_{PAEK}^{out}
PSP_{14}-*b*-$PAEK_{14}$	0.132	0.068	0.188	0.279	0.32	0.133
PSP_{28}- *b*-$PAEK_{14}$	0.026	0.434	0.044	0.286	0.07	0.14